Title: High-risk microbial signatures are associated with severe parasitemia in controlled *Plasmodium* infections of both humans and rhesus macaques

Authors: Andrew T. Gustin[1,2], Courtney A. Broedlow[1,2,3], Ernesto Coronado[2,3], Solomon Wangari[2], Naoto Iwayama[2], Chul Y. Ahrens[2], William D. Garrison[2], Kathryn A. Guerriero[2,5], Kristina DeParis[6], Michael Gale, Jr.[1,2], Nichole R. Klatt[2,3,4], James G. Kublin[7], Jennifer A. Manuzak[2,3,8,9]

Affiliations:

[1]Department of Immunology, University of Washington, Seattle, WA, USA

[2]Washington National Primate Research Center, University of Washington, Seattle, WA, USA

[3]Department of Pharmaceutics, University of Washington, Seattle, WA, USA

[4]Division of Surgical Outcomes and Precision Medicine Research, Department of Surgery, University of Minnesota, Minneapolis, MN, USA

[5]Division of Veterinary Resources, National Institutes of Health Animal Center, Poolesville, MD, USA

[6]Department of Microbiology and Immunology, University of North Carolina School of Medicine, Chapel Hill, NC, USA

[7]Seattle Malaria Clinical Trials Center, Fred Hutchinson Cancer Research Center, Seattle, Washington, USA

[8]Division of Immunology, Tulane National Primate Research Center, Tulane University, Covington, LA, USA

[9]Department of Microbiology and Immunology, Tulane University School of Medicine, New Orleans, LA, USA

***Corresponding author:**

Jennifer A. Manuzak

Assistant Professor

Division of Immunology

Tulane National Primate Research Center

29 Department of Microbiology and Immunology
30 Tulane University School of Medicine
31 18703 Three Rivers Road
32 Covington, LA, 70433
33 jmanuzak@tulane.edu
34
35 **Alternate corresponding author:**
36 Andrew T. Gustin
37 Postdoctoral scholar
38 Department of Immunology
39 University of Washington School of Medicine
40 750 Republican St.
41 Seattle, WA 98101
42 atgustin@uw.edu
43

44 **Abstract**

45 While functions of the gastrointestinal (GI) microbiome include maintenance of immune homeostasis and
46 protection against infectious disease, its role in determining disease severity during *Plasmodium* infection
47 has been limited to mouse models and observational human cohorts. Here, we performed controlled
48 *Plasmodium* infection in both humans and rhesus macaques (RMs) to experimentally determine the
49 impact of GI microbiome composition on disease progression. Through analysis of serially collected
50 microbiome samples, we identified a high-risk microbial signature that strongly associated with increased
51 risk of developing severe parasitemia in human participants. Importantly, we identified a parallel
52 phenomenon in RMs. The combined weight of this evidence demonstrates that pre-infection GI
53 microbiome composition is highly indicative of *P. falciparum* disease risk. Moreover, our observation that
54 *P. fragile*-microbiome dynamics in RMs closely mirrors *P. falciparum*-microbiome interactions in humans
55 strongly supports the use of this model in pre-clinical investigations of novel microbiome-targeting
56 approaches to reduce malaria burden.

57

58 **Introduction**

59 Despite effective prevention and treatment measures, infection with *Plasmodium*, the causative agent of
60 malaria, remains a significant global public health burden. Current World Health Organization estimates
61 indicate over 241 million cases of malaria worldwide in 2020, with over 627,000 deaths due to malaria
62 infection[1]. Notably, in addition to the classic clinical features of fever and anemia, *P. falciparum* malaria
63 has been shown to induce gastrointestinal manifestations, including abdominal pain, diarrhea, and
64 vomiting[2]. Moreover, previous work has demonstrated that elevated parasite sequestration occurs in the
65 intestine during *Plasmodium* infection in both mice and humans[3-6], and that damage to the blood vessels
66 due to parasite sequestration could contribute to disruptions in gastrointestinal morphology and function,
67 including altered villi formation[7], increased gastrointestinal permeability[7,8], and increased malabsorption[9-
68 11]. These alterations may contribute to the higher levels of microbial translocation that have been
69 observed during *Plasmodium* infection[8,12-15], including dissemination of nontyphoidal salmonella
70 (NTS)[16,17]. However, the precise biological mechanisms underlying *Plasmodium*-induced gastrointestinal
71 disruptions remain poorly defined.

72

73 GI microbes play an essential role preserving epithelial barrier integrity and maintaining appropriate
74 immune surveillance, and suboptimal microbial consortiums in the GI tract have been shown to influence
75 acquisition of several enteric pathogens[18]. Interestingly, several lines of evidence indicate that GI
76 microbiome community structure may be linked with protection against severe *Plasmodium* infection. For
77 example, recent work conducted among Ugandan children demonstrated significant differences in alpha-
78 diversity measures of fecal bacterial composition, including Shannon index and community evenness
79 (Pielou) between participants with severe malaria anemia and participants with asymptomatic *P.*
80 *falciparum* infection or healthy controls, which suggests a link between intestinal microbial community
81 structure and the severity of *Plasmodium* infection[19]. Additionally, a study conducted among children in
82 Mali demonstrated that participants with higher stool abundances of *Bifidobacterium* and *Streptococcus*
83 species had a statistically significant delay in time to *P. falciparum* infection, as compared to participants
84 with greater abundances in *Ruminococcaceae* and *Lachnospiraceae*, suggesting an association between

85 specific GI microbiome composition and decreased prospective risk for *Plasmodium* acquisition[20]. Murine
86 studies have also provided evidence that higher intestinal abundances of *Lactobacillus* and
87 *Bifidobacterium* can be associated with reduced parasite burden following *P. yoelii* challenge[21].
88 Moreover, decreased abundance of *Lactobacillaceae* was inversely correlated with *P. berghei* ANKA
89 parasite burden, while increased abundances of *Enterobacteriaceae* and *Verrucomicrobicaeae* were
90 positively corelated with parasitemia[22]. Finally, differences in intestinal microbial communities between
91 mice that were resistant or susceptible to *P. yoelii* infection were associated with differences in the
92 magnitude of spleen germinal center responses, particularly the quality and specificity of anti-
93 *Plasmodium* antibodies, thereby providing a potential mechanism by which the intestinal microbiome
94 could influence the severity of *Plasmodium spp.* infection[23]. Taken together, these findings support the
95 theory that the pre-existing intestinal microbiota composition may influence both the prospective risk for
96 and severity of *Plasmodium* infection.
97
98 While observational studies have suggested a link between microbiota composition and the prospective
99 risk for and severity of *Plasmodium* infection, there remains a critical need for controlled human malaria
100 infection (CHMI) studies to determine the role of the microbiome in shaping the outcome of *Plasmodium*
101 infection. Such studies will be important for determining whether the previous cross-sectional and
102 prospective observational findings in human children and infants are broadly applicable across age
103 ranges. Additionally, a representative animal model is required to assess mechanistic relationships
104 between *Plasmodium* infection and GI microbiota, intestinal inflammation, and mucosal epithelial barrier
105 integrity. While existing mouse models have provided useful insights, intervention-based studies will likely
106 require a non-human primate (NHP) model to assess the translational potential of microbiota
107 manipulation on malaria severity. Here, we present evidence from controlled malaria infection studies in
108 both humans and NHPs that (1) confirms a strong relationship between the pre-infection GI microbiota
109 composition and the potential for severe malaria; and (2) demonstrates that NHP are an ideal animal
110 model for basic and translational investigations of microbiome-*Plasmodium* interactions.
111
112 **Materials and Methods**

113 Controlled human malaria infection (CHMI) study and approval

114 Healthy adult participants were enrolled in a nonconfirmatory, 2-part, randomized, double-blinded,
115 placebo-controlled, single-center study completed at the Seattle Malaria Clinical Trials Center to test the
116 prophylactic efficacy, safety, and pharmacokinetics of KAF156, a novel imidazolopiperazine class of
117 antimalarial drug (clinical trials registration number: NCT04072302)[24]. As reported previously, KAF156
118 was found to be safe, well-tolerated, and resulted in a high degree of protective efficacy from *P.*
119 *falciparum* infection, which was tested through a controlled human malaria infection (CHMI) model[24]. A
120 subset of participants that received either placebo (n=8), 20mg (n=13), or 50mg (n=14) of KAF156 post-
121 CHMI exposure to *P. falciparum*-infected mosquitoes also provided stool samples at four distinct time
122 points: (1) Within 1-2 days of CHMI; (2) during a three-day course of treatment with the antimalarial drug
123 Malarone (atovaquone/proguanil); (3) at the end of Malarone treatment; and (4) during CHMI and
124 treatment follow-up (within D28 – D42). *P. falciparum* infection in study participants was monitored in
125 whole peripheral blood using a *Plasmodium* 18S ribosomal RNA (rRNA) qRT-PCR that quantified Pf A-
126 type 18S rRNA[24-26]. Stool samples were frozen at -80°C within 24hours of collection. Upon thawing, DNA
127 was extracted from human stool samples and used for 16s rRNA sequencing analysis, as detailed below.
128

129 Nonhuman primate study animals, approval, and sample collection

130 Sixteen male Indian-origin rhesus macaques (*Macaca mulatta*; RMs) were utilized in this study. All RMs
131 were housed and cared for at the Washington National Primate Research Center (WaNPRC) under a
132 protocol that was reviewed and approved by the University of Washington Office of Animal Welfare
133 (OWA) Institutional Animal Care and Use Committee (IACUC; Protocol 4266-13; Animal Welfare
134 Assurance Number D16-00292). The housing, care, and procedures performed in this study were done
135 in an AAALAC-accredited facility, in accordance with the regulations put forth by the United States
136 Department of Agriculture, including the Animal Welfare Act (9 CRF) and the Animal Care Policy Manual,
137 as well as with the guidelines outlined by the National Research Council in the Guide for the Care and
138 Use of Laboratory Animals and the Weatherall Report. All RMs were provided with a commercial primate
139 chow (Lab Diet, PMI Nutrition International, St. Louis, MO) twice per day, supplemented with daily fruits
140 and vegetables and water ad libitum. Novel food items, foraging opportunities and destructible and

141 indestructible manipulanda were provided as environmental enrichment. All RMs were housed in
142 stainless steel cages with a 12/12 light cycle. All cage pans and animal rooms were cleaned daily and
143 sanitized at least every two weeks. Stool was collected from each RM two weeks prior to *P. fragile*
144 inoculation (Week -2), the day of *P. fragile* inoculation (Week 0), and during *P. fragile* infection and
145 treatment (Weeks 1, 2, 3, 4 and 6). The evening prior to stool collection, RMs in full social contact were
146 shifted into protected (grooming) contact only. The following morning, stool was collected from each
147 animal's cage pan and immediately stored at -80°C. Following cage pan stool collection, RMs were
148 returned to full social contact. Upon thawing, DNA was extracted from NHP stool samples and used for
149 16s rRNA sequencing analysis, as detailed below.
150
151 <u>*P. fragile* inoculation, post-infection monitoring, and treatment</u>
152 *P. fragile*-infected RM erythrocytes were prepared as previously described[27]. Briefly, frozen erythrocytes
153 from a *P. fragile*-infected RM were thawed rapidly at 37°C and transferred into a sterile tube. Erythrocytes
154 were resuspended in 12% NaCl while gently shaking, followed by a 5min incubation at room temperature
155 without shaking. Next, 1.6% NaCl was added dropwise while gently shaking, followed by centrifugation
156 at 1400RPM, room temperature, 10min. After centrifugation, the supernatant was aspirated and
157 discarded, and the pellet resuspended in a solution of 0.9% NaCl and 2% dextrose, followed by
158 centrifugation at 1400RPM, room temperature, 10min. After the second centrifugation, the supernatant
159 was aspirated and discarded, and the pellet resuspended in 0.9% NaCl solution. Finally, RMs were
160 intravenously inoculated with up to 20x10^6 *P. fragile*-infected erythrocytes in 1ml 0.9% NaCl solution.
161
162 Giemsa staining of thin blood smears was used to assess *P. fragile* parasitemia in each RM. Parasitemia
163 checks occurred three times per week following *P. fragile* inoculation, with an additional check occurring
164 at week 6 post-*P. fragile* infection. Parasitemia was quantified using a light microscope and 1:10 ratio
165 Miller Disk Reticle (Microscope World, Carlsbad, CA), as previously described[28]. Briefly, the total number
166 of all red blood cells (RBCs), including both infected RBCs (iRBCs) and non-infected RBCs, inside the
167 minor square are enumerated, followed by counting of all iRBCs in the major square. A total of fifteen
168 fields were counted in three separate areas of the slide, for a total of 45 fields. The % parasitemia was

169 calculated in each of the three areas as follows: (# of iRBC in major square / # of all RBC in minor square)
170 x 10. The % parasitemia in each of the three areas was then averaged together to determine the final %
171 parasitemia for each RM at each timepoint.
172
173 The % parasitemia at each time point was used to determine the need for anti-malarial treatment. RMs
174 were treated using the following guidelines: if parasitemia was between 0.5-1%, RMs were treated orally
175 with quinine sulfate (150mg) once per day. If parasitemia was above 1%, RMs were treated orally with
176 quinine sulfate twice per day. If parasitemia was above 0.5% for two consecutive weeks, RMs were
177 switched to oral chloroquine treatment (10-20mg/kg) once per day. Quinine sulfate and chloroquine
178 treatments were halted as soon as RMs were observed to be below the 0.5% parasitemia threshold.
179
180 16s rRNA sequencing
181 DNA was extracted from both NHP and human stool samples using the PowerFecal DNA Isolation Kit
182 (Qiagen, Valencia, CA). Sequencing libraries were constructed using Earth Microbiome Protocols for 16s
183 sequencing[29]. The following primers were used to sequence the V4 region of the 16s small subunit
184 ribosomal ribonucleic acid (SSU rRNA): 515F (5′-GTGYCAGCMGCCGCGGTAA-3′) – 806R (5′-
185 GGACTACNVGGGTWTCTAAT- 3′), as previously described[30]. PCR amplification was performed in
186 triplicate, after which amplicon products were normalized, pooled, cleaned, and quantified (KAPA
187 quantification, KAPA Biosystems, Wilmington, MA). An Illumina MiSeq (MiSeq Control Software,
188 including MiSeq Reporter, version 3.1) was used to sequence the library with a 2x150 bp cycle with 20%
189 PhiX phage as a control. All raw sequence data have been deposited in the NCBI SRA (Accession
190 number pending).
191
192 Bioinformatics and statistical analysis
193 16S rRNA amplicon sequencing reads were demultiplexed in Illumina Basespace. Fastq files were
194 assessed for read quality, trimmed (trimLeft=12, truncLen=150), dereplicated, and filtered using the
195 dada2 pipeline in R studio. Following removal of chimeric sequences, reads were assigned a taxonomy
196 using greengenes (gg_13_8_train_set_97.fa.gz) and a phylogenetic tree was built using MSA and

197 Phangorn. The reads, metadata, and tree were then combined into a phyloseq object for additional quality
198 controls and filtering, which included removing ASVs mapping to mitochondria, chloroplast and
199 cyanobacteria reads, as well as any ASV detected in only one sample. The resulting phyloseq object was
200 used for all downstream analyses.
201
202 Unsupervised hierarchical clustering was conducted on center log ratio (CLR)-transformed read counts,
203 using a divisive approach (Cluster::diana). The same CLR-transformed read counts were used to
204 visualize human reads in PCA space. Alpha diversity was calculated using the microbiome package to
205 assess raw reads. Prevalence, proportion tests, and CLR-transformed abundances were assessed using
206 custom scripts that are available upon request. Differential abundance was performed using DESeq2 to
207 assess raw reads on genera-level objects generated using phyloseq::tax_glom. Time course data were
208 smoothed using default options for ggplot2::geom_smooth. PCoA of RM samples were generated by first
209 running phyloseq::ordinate on the phyloseq object, and the resulting objects were visualized using
210 phyloseq::plot_ordination. All code is available upon request. Log2 peak parasite burdens, Shannon
211 diversity levels, and CLR-transformed counts were compared using a pairwise Wilcoxon test. Significant
212 differences in prevalence were assessed by proportion test. Differential abundances were determined
213 using DESeq2 with a Wald test.
214
215 **Results**
216 Pre-infection composition of the human intestinal microbiome is significantly associated with parasite
217 burden during controlled malaria infection
218 To confirm previous reports from human observational and murine studies that suggested an association
219 between baseline microbiota and potential for severe malaria, we first assessed the stool microbiota in a
220 cohort of 35 healthy adults participating in a CHMI study[24]. As previously reported, of the 35 participants
221 inoculated via infected mosquito bite, 32 progressed to detectable parasitemia by qPCR[24]. The
222 antimalarial treatment Malarone (atovaquone/proguanil) was subsequently initiated according to a
223 predetermined criteria of two consecutive positive qRT-PCR test results, with at least one measurement
224 greater than 250 parasites/ml[24]. Stool samples were collected from study participants (1) prior to

225 challenge, (2) at peak parasitemia (prior to antimalarial treatment thresholds), (3) post-treatment, and (4)
226 during follow-up (Fig. 1A).
227
228 We began our study with the primary hypothesis that the magnitude of parasite burden following
229 *Plasmodium* challenge would vary according to microbiota composition. To test this hypothesis, we
230 performed unsupervised, divisive hierarchical clustering on the 16S rRNA sequencing data to identify
231 major community types. This analysis demonstrated that participants' baseline microbiota compositions
232 could be segregated into three distinct clusters (Fig.1B). To determine whether the odds of developing
233 high parasitemia levels differed amongst participants in each of the three microbiome clusters, we ranked
234 participants according to their peak parasite burden and then categorized each participant's outcome as
235 either mild or severe parasitemia, defined as having parasite burden above or below the median
236 parasitemia value, respectively. Participants in human microbiome cluster 1 (HC1; pink) were more than
237 eight times as likely to experience high parasite burden as compared to participants in HC3 (green; OR
238 = 8.17, 95% CI = 7.11 - 9.22), while participants grouped in HC2 (brown) were more than four times as
239 likely to develop high parasitemia as compared to HC1 (OR = 4.08, 95% CI = 3.10 – 5.06) (Fig. 1C).
240 Given that baseline microbiota composition was associated with the odds of developing more severe
241 parasitemia, we next directly assessed the parasite burden for each cluster. Participants in HC1
242 developed significantly higher levels of parasitemia as compared to participants in HC3 (p=0.043); HC1
243 peak parasitemia was also elevated compared to HC2, although this difference did not reach statistical
244 significance (p=0.17; Fig. 1D). Parasite burden was also observed to be non-significantly elevated in
245 participants in HC2 compared to HC3 (p=0.23; Fig. 1D). Taken together, these findings demonstrated
246 that baseline microbiota composition was strongly associated with parasite burden during controlled
247 *Plasmodium* infection in humans.
248
249 <u>Human intestinal microbiome composition is robustly associated with malaria severity and progression</u>
250 Having observed a significant difference in potential for severe infection across microbiota clusters, we
251 next assessed the composition of the three major microbiota clusters to identify structural and
252 compositional distinctions. To begin, we performed principal components analysis (PCA) on all collected

253 timepoints and found that while participants assigned to HC1 were widely dispersed in PCA space,
254 participants from HC2 were only modestly dispersed and those from HC3 were tightly clustered (Fig. 2A
255 and B), indicating greater variability in microbial composition in HC1 as compared to HC2 or HC3. These
256 patterns were especially evident with information from the third principal component added in 3-
257 dimensional space (Fig. S1). We next considered samples from baseline only and found that while
258 samples from HC2 and HC3 had significant overlap along PC1 and minimal spread along PC2, samples
259 from HC1 demonstrated higher variability along both PC axes (Fig. 2C and D). Taken together, these
260 results affirmed the hierarchical cluster assignments by illustrating the degree to which HC1 differed from
261 HC2 and HC3 in terms of both composition and variability at baseline alone, as well as throughout *P.*
262 *falciparum* infection.
263
264 We next asked if within-sample alpha diversity was a distinguishing aspect of cluster identities. To do so,
265 we first assessed the cumulative number of unique amplicon sequence variants (ASVs) that were
266 detected at any time in each microbiota cluster. We observed that the number of unique ASVs in HC1
267 (n=762) were almost two-fold greater than the number of unique ASVs in HC3 (n=488; Fig. 2E), indicating
268 that a greater range of taxa were detected in HC1 and explaining the wide dispersion of samples from
269 this cluster in PCA space. Given this large separation in taxonomic diversity, we next calculated Shannon
270 diversity scores for all samples, which assesses both sample richness, characterized as the total number
271 of observed ASVs, and evenness, which indicates the balance of reads amongst ASVs. Shannon
272 diversity scores for HC1 samples were elevated as compared to those in HC2, a finding that remained
273 stable across all measured time points and was statistically significant at baseline, post-treatment, and
274 follow-up (p=0.0011, 0.047, and 0.026, respectively; Fig. 2F). Likewise, measured Shannon diversity for
275 samples from HC1 were consistently elevated compared to HC3 and were significantly higher at the
276 baseline and follow-up time points (p=0.0021 and 0.00097, respectively; Fig. 2F). Shannon diversity
277 scores for participants in HC2 and HC3 were similar over time, with the exception of the follow-up time
278 point, at which HC2 showed significantly higher scores than HC3 (p=0.025; Fig. 2F). Given our
279 observation that participants in HC1 had significantly higher parasite burden as compared to HC2 and
280 HC3 participants, these findings suggested a link between increased microbiota diversity and

281 development of higher parasite burdens; additionally, the consistency of these results over time also
282 suggest pre-existing community structure is reestablished following transient changes in community
283 structure induced by *Plasmodium* infection.
284
285 To further validate the potential relationship between microbiota diversity and parasite burden throughout
286 infection, we assessed Shannon diversity profiles of participants that were split based on severe versus
287 mild parasitemia. Our results demonstrated that participants who experienced the highest levels of
288 parasitemia had consistently higher Shannon diversity as compared to participants in with only mild
289 parasitemia (Fig. 2G). This difference was statistically significant pre-challenge ($p=0.027$) and trended
290 towards significance at the follow-up time point ($p=0.054$; Fig. 2G). Additional linear regression analysis
291 further suggested a link between measured diversity and peak parasite loads, though these findings did
292 not reach significance (Fig. S2; $p=0.0875$). Taken together, the strong relationship between increased
293 microbiota diversity and higher parasite loads indicated that elevated diversity in the GI microbiota of
294 participants prior to *Plasmodium* challenge could contribute to the development of high parasitemia
295 during *P. falciparum* infection.
296
297 <u>Genus-level distinctions in human intestinal microbial composition are linked with malaria disease</u>
298 <u>severity and progression</u>
299 We next hypothesized that the increased microbial richness detected in HC1 participants would result in
300 reduced detection and measured abundance of core ASVs as compared to participants in HC3. To test
301 this hypothesis, we measured the prevalence of all ASVs detected in at least one third of all participant
302 samples from all time points and subsequently performed proportionality tests for HC1 versus HC3. We
303 observed that highly prevalent ASVs, defined as ASVs detected in more than 75% of all samples, were
304 consistently detected at lower frequencies in participants from HC1 as compared with HC3 (Fig. 3A).
305 Conversely, ASVs with lower overall prevalence were more likely to be detected in HC1 than HC3.
306 Amongst the ASVs that were observed to be differentially prevalent between HC1 and HC3, we identified
307 several key GI microbiota that were significantly less prevalent in the microbiomes of HC1 participants,
308 including ASVs for *Bifidobacterium longum* ($p<0.0005$), *Bifidobacterium adolescentis* ($p<0.005$), and

309 *Akkermansia muciniphila* ($p<0.005$; Fig. 3A). Thus, our data indicate that core GI microbiota ASVs are
310 less prevalent in HC1 participants, who are also more likely to develop severe parasitemia, and that their
311 absence is accompanied by the increased detection of low prevalence taxa.
312
313 Given our observation that ASVs that were frequently detected in HC3 participants with mild parasitemia
314 were less likely to be detected in HC1 participants who developed severe parasitemia, we next assessed
315 whether the abundances of core taxa, when detected, were different between participant groups. To
316 evaluate this question, we compared center log ratio (CLR)-transformed count data for the 20 most
317 prevalent taxa between HC1, HC2 and HC3 participants. We observed that the majority of highly
318 prevalent ASVs were significantly less abundant in participants from HC1 as compared to HC2 and HC3
319 (Fig. 3B). The application of strict Bonferroni corrections demonstrated the strong significance within
320 these findings and highlighted reduced levels of *Bifidobacterium adolescentis* ($p=0.00069$; Fig. 3B),
321 among others. Taken together, our data demonstrate that participants who developed high parasite
322 burdens harbored lower abundances of core GI microbiota, and that these findings were robust even
323 when accounting for decreased prevalence of these same taxa.
324
325 To determine whether the risk for progression to severe malaria after challenge was driven by high-level
326 differences in community composition at baseline, we performed differential abundance analysis on all
327 pre-challenge samples at the genus level. Our analysis demonstrated that participants in HC1 likely to
328 develop severe parasitemia had reduced levels of *Megamonas*, *Streptococcus, and Bifidobacterium*
329 relative to participants in HC2 and HC3 ($p=0.0037$, 0.01, and 0.0067, respectively) and that these
330 reductions were balanced by increased levels of several genera that included *Escherichia,*
331 *Catenibacterium,* and *Peptoniphilu*s ($p=0.0016$, 0.0000, and 0.0031, respectively; Fig. 3C). Closer
332 examination of these results again highlighted that HC1 participants had significantly lower abundances
333 of widely detected genera like *Bifidobacterium* and *Streptococcus*, which were amongst the most
334 abundant taxa in participants from HC2 and HC3 (Fig. 3D and E). Conversely, several rarely detected
335 genera, such as *Megamonas*, *Escherichia*, and *Catenibacterium,* were observed at high abundances
336 (Fig. 3F - H). This pattern was far more common in HC1, a finding that explains the wide dispersion of

337 HC1 samples in PCA space (Fig.2A) and highlights the degree to which participants within HC1 differed
338 from one another.
339
340 To place these pre-challenge findings in context, we concluded our analyses of the human cohort by
341 examining the stability of differentially abundant genera throughout infection. We observed that levels of
342 both *Megamonas* and *Bifidobacterium* remained consistently elevated in HC3 throughout the study, while
343 *Blautia* and *Streptococcus* remained consistently highest in HC2, with HC3 approaching similar levels
344 (Fig. 3I). These findings demonstrate the stability of these genera in participants who developed only mild
345 parasitemia. Conversely, levels of *Catenibacterium*, *Megasphaera*, *Peptoniphilius*, and *WAL_1855D*
346 were consistently elevated in HC1 (Fig. 3I), indicating a potential association with risk for severe malaria.
347 Finally, levels of *Escherichia* and *Roseburia* were found to be disrupted following challenge, and although
348 *Escherichia* did return to pre-challenge levels in each of the three community clusters, *Roseburia* was
349 observed to be consistently diminished in HC3 following infection. Taken together, these findings suggest
350 that high-level distinctions between microbiota clusters contribute to risk for malaria severity, and that GI
351 microbial communities are generally stable subsequent to *P. falciparum* infection.
352
353 <u>Distinct microbial cluster identified within the RM intestinal microbiome is significantly associated with</u>
354 <u>parasite burden during P. fragile infection</u>
355 To further test our hypothesis that the GI microbiome plays a direct role in *Plasmodium* progression, we
356 conducted experimental infection of rhesus macaques (RMs) with *P. fragile*, a macaque *Plasmodium*
357 previously shown to induce clinical signs in RMs comparable to those caused by *P. falciparum* in
358 humans[31-33]. To assess the microbiota, we characterized stool microbial communities of male RMs (n=16)
359 over a time course that spanned two weeks prior to *P. fragile* challenge through six weeks post-infection
360 (Fig. 4A). We first stratified the animals according to their pre-challenge microbiota, using the same
361 unsupervised hierarchical clustering approach employed with the human microbiome data (Fig. 4B). In
362 RMs, microbiome compositions were split into two major branches, hereafter referred to as macaque
363 cluster 1 and 2 (MaC1 and MaC2, respectively). As with the human participants, we performed a median
364 split based on peak parasite levels of all RMs and categorized RMs as either progressing to mild or

365 severe parasitemia. When malaria severity data were viewed in the context of microbiome clusters, we
366 identified that RMs in MaC1 were nine times as likely to develop high parasite loads as RMs in MaC2
367 (OR = 8.75, 95%CI = 7.59-9.91). Moreover, RMs in MaC1 reached peak parasite loads nearly three times
368 greater than RMs in MaC2 (p=0.003; Fig. 4C). Thus, the pre-infection microbiota composition of RMs
369 was associated with the likelihood of developing severe malaria, similarly to human CHMI participants.
370

371 RMs with distinct intestinal microbial composition have greater risk of developing severe malaria

372 We next assessed RM microbiota clusters using alpha and beta diversity approaches. To define
373 differences between clusters, we first analyzed all RM samples from all timepoints in PCA space. As with
374 CHMI data, PCA analyses reiterated the clear linkage between microbiota composition and malaria
375 progression that was established during hierarchical analysis (Figs. S3A and B). However, unlike human
376 participants, these distinctions could not be explained by differences in alpha diversity. Indeed,
377 measurements of Shannon diversity indicated no significant differences between microbiome clusters at
378 any timepoint, nor were differences observed when assessing Shannon diversity according to parasite
379 burden (Fig. S3C and D). These data suggested that the distinctions between RM microbiota clusters
380 may not be driven by the same differences in microbial community organization that were observed
381 across human clusters. Therefore, we sought to expand our analysis by using a canonical microbiome
382 distance metric that accounted for compositional differences by determining the proportion of each
383 sample that was unique relative to other samples and weighting these results according to abundance
384 data. This weighted-UniFrac metric captured over 60% of the variance in the first two axes and
385 demonstrated not only that MaC1 clustered separately from MaC2 (Fig. 5A), but that these hierarchically
386 assigned microbial clusters were associated with distinct differences in parasite burden (Fig. 5B).
387 Faceting data according to timepoint that the microbial communities of RMs assigned to either MaC1 or
388 MaC2 based on pre-challenge microbial profiles remained distinct following recovery from *P. fragile*
389 infection (Fig. 5C). Notably, despite this overall stability, samples from week 3 post-challenge were not
390 distinct in PCoA space, suggesting that while microbial communities may be relatively resistant to
391 influence from *P. fragile* infection, they may be transiently disrupted during the course of the infection
392 (Fig. 5C). Taken together, our alpha and beta diversity assessments suggested that the separation of the

393 two microbiota clusters was not driven primarily by differences in richness or evenness, but rather, that
394 these clusters were stratified by compositional differences.
395
396 Genus-level distinctions in RM intestinal microbial composition are linked with malaria disease severity
397 and progression
398 We next proceeded to assess differences in prevalence and abundance between RMs in MaC1 and
399 MaC2. As with CHMI data, we measured the abundance of core ASVs present in at least one third of all
400 samples for each microbiota cluster and performed proportionality tests for MaC1 versus MaC2 (Fig.6A).
401 We found that ASVs from the *Prevotella* genus and *Ruminococcaea* family were more likely to be present
402 in MaC2, where RMs were more likely to experience only mild parasitemia (Fig. 6A). Conversely, RMs
403 assigned to MaC1, which were more likely to develop severe parasitemia, more frequently carried ASVs
404 from the *Lachnospiraceae* family, and the *Lactobacillus* and *Treponema* genera (Fig. 6A). We next
405 assessed whether these highly prevalent ASVs differed in abundance in samples where they were
406 detected and found that the majority of core ASVs had abundances that were relatively similar between
407 MaC1 and MaC2. Two important exceptions were the elevated abundance of several *Prevotella* ASVs in
408 MaC2 RMs, which were countered by significant elevations of *Lactobacillus* ASVs in MaC1 RMs (Fig.
409 6B). To assess for cumulative differences in ASVs, we combined all genus level data and tested for
410 differentially abundant genera on the day of inoculation. We identified 16 genera whose abundances
411 differed significantly between MaC1 and MaC2 (Fig.6C). Interestingly, the *Prevotella* genus was found to
412 be significantly elevated prior to challenge in MaC2 RMs (Fig.6D), whereas MaC1 RMs, which were more
413 likely to develop severe parasitemia, had elevated baseline levels of *Ruminococcus*, *Treponema*, and
414 *Sphaerochaeta*, amongst others (Fig. 6E). Finally, we concluded our RM assessment by examining the
415 stability of these differentially abundant communities over the course of the study (Fig. 6F). We observed
416 that the pre-challenge elevation in *Prevotella* abundance in MaC2 was maintained over time (Fig. 6F).
417 These findings suggested a beneficial role of the *Prevotella* genus in the context of *Plasmodium* infection,
418 as reduced levels were consistently associated with the risk of severe parasitemia. Other genera shown
419 to be significantly different pre-challenge had abundances that varied widely throughout the course of *P.*
420 *fragile* infection, with ratios between MaC1 and Mac2 frequently inverted during weeks 1 - 3 post-infection

421 (Fig. 6B), the time period during which parasite levels were highest (Fig. S4). This observation agrees
422 with our week-by-week breakdown of unifrac distances (Fig. 5C) and further indicates that *P. fragile*
423 infection may disrupt the GI microbiome in RMs. Notably, although abundances of several genera were
424 disrupted following *P. fragile* infection, the majority returned to pre-infection levels by 6 weeks post-
425 challenge and thereby reestablished the distinction between MaC1 and MaC2 clusters. Taken together,
426 these data highlight that, like humans, RMs possess natural variation in their GI microbiota that appears
427 to predispose a portion of the population to more severe *P. fragile* infection when exposed.
428

429 **Discussion**

430 In this study, we leveraged controlled malaria infection of both humans and NHPs to test the hypothesis
431 that the composition of GI tract microbiota prior to *Plasmodium* challenge influences the severity of
432 malaria infection. Analysis of samples from our CHMI study indicated that baseline microbiota
433 composition in the human GI tract was strongly associated with the potential for severe *P. falciparum*
434 infection. Specifically, after using unsupervised analysis to identify three community-type clusters, we
435 determined that participants in HC1 were nearly nine times as likely to develop severe parasitemia as
436 participants in HC3, with parasite burdens that were nearly six times greater. Downstream analyses
437 indicated that key GI microbes, including *Bifidobacterium longum*, *Bifidobacterium adolescentis*, and
438 *Akkermansia muciniphila* were detected less frequently and at lower abundances in participants that were
439 more likely to develop severe parasitemia. Our findings extend previous observations made in the murine
440 model[21-23], as well as observational studies using incident detection in human children living in malaria
441 endemic areas[19,20], both of which suggested a link between GI microbiome composition and the risk of
442 developing severe malaria infection. Importantly, our work extends these observations to adult humans
443 and highlights *Bifidobacterium* as a defining microbial feature in determining risk for severe *P. falciparum*
444 parasitemia. The agreement between these studies is made more impressive when considering that our
445 CHMI study was performed on a malaria-naïve cohort of adult individuals in Seattle, Washington,
446 whereas the previous observational studies identifying links between microbial composition and *P.*
447 *falciparum* infection risk were conducted among infants and children located in rural West Africa, where
448 malaria incidence is seasonal. Taken together, these differences highlight the robust nature of our

449 findings and position *Bifidobacterium* as a key taxon for future studies aimed at mitigating malaria severity
450 in endemic regions.
451
452 Our analyses demonstrated that major distinctions in GI microbiota organization at multiple taxonomic
453 levels distinguished human participants who were more likely to develop high parasite levels following *P.*
454 *falciparum* infection. In particular, we observed that the absence of *Bifidobacterium* and other core taxa
455 in CHMI participants grouped in HC1 was balanced by an increase in the prevalence and abundance of
456 ASVs that were less common in participants that developed only mild parasitemia. This finding was
457 further highlighted by the significantly higher number of detected ASVs in HC1 participants as compared
458 to HC2 and HC3 participants. This strong relationship between increased microbiota diversity and higher
459 parasite loads suggests that an aspect of elevated diversity in the GI microbiota prior to *P. falciparum*
460 exposure could contribute to the development of high parasitemia during infection. Mechanistically, the
461 loss or reduction of key commensals such as *Bifidobacterium* and *Akkermansia* could result in
462 inappropriate or inadequate priming of the host immune due to disruptions in beneficial, low-level immune
463 stimulation[34-37]. Alternatively, their displacement by an expansion of uncommon taxa could disturb
464 metabolic networks in the GI tract and subsequently promote pathologic changes to the GI barrier[38]. In
465 either hypothetical, host immune disruptions could manifest both locally and systemically in such a way
466 as to promote *Plasmodium* replication following infection. It is also important to consider that microbial
467 composition may serve as a proxy for an indirectly related facet of overall health that ultimately plays a
468 larger role in malaria progression, although the identification of the same phenomenon in RMs argues
469 against this. Finally, although unlikely, it is possible that microbiome constituents directly impact the
470 *Plasmodium* lifecycle. Taken together, future investigations to determine the precise mechanisms by
471 which GI microbiota composition influences the severity of *P. falciparum* infection in humans are
472 warranted.
473
474 A critical observation from our study is that similarly to humans, GI microbiota composition in RMs was
475 significantly associated with the potential for severe *P. fragile* infection. Indeed, unsupervised clustering
476 delineated two major RM GI microbiome community types prior to challenge. RMs that possessed higher

477 levels of ASVs from the *Lachnospiraceae* family, and the *Lactobacillus* and *Treponema* genera were
478 more likely to have severe *P. fragile* parasitemia, while RMs with ASVs from the *Prevotella* genus and
479 *Ruminococcaea* family were more likely to develop only mild parasitemia. Unlike the CHMI participants,
480 the RM microbiota clusters we identified were not defined by the presence or absence of rare taxa.
481 Instead, significant distinctions between groups were primarily detected as differences in the abundance
482 of core taxa. Notably, in both humans and RMs, while it appeared that GI microbiome was generally
483 resilient to transient changes that occurred during *Plasmodium* infection, our data showed that disruptions
484 mainly occurred near peak parasitemia. Moreover, in RMs *Prevotella* was the only genera where
485 differences in pre-challenge levels between MaC1 and MaC2 were maintained throughout the study,
486 suggesting that ASVs within this genus have a stable niche space that is somehow diminished in RMs
487 likely to develop severe parasitemia. These findings are consistent with previous work conducted among
488 Kenyan infants, which revealed only minimal differences in stool community structure and composition
489 before and after episodes of *P. falciparum* infection and artemether-lumefantrine treatmen[39]. Conversely,
490 previous murine work has suggested that *P. yoelli* infection results in decreased abundance of Firmicutes
491 and increased abundance of Bacteroidetes[5,40], while *P. berghei* ANKA infection results in decreased
492 Bacteroidetes and Verrucomicrobia phyla, but substantially increased Firmicutes and Proteobacteria
493 following infection[41,42]. Taken together, the striking degree to which these RM GI microbiome findings
494 agreed with data from CHMI participants and prior observational studies in human children supports our
495 hypothesis that microbiome composition is a significant determining factor in *Plasmodium* infection.
496 Moreover, our findings further indicate the significant translational potential of the *P. fragile* RM model of
497 *P. fragile* infection. Given the additional strong similarities between RMs and humans in terms of GI
498 functionality and mucosal immunity, future studies utilizing this model to investigate the impact of *P.*
499 *fragile*-mediated GI microbiome disruptions on intestinal mucosal barrier integrity and malaria disease
500 progression are justified.
501
502 A major strength of our study was the use of the RM model, which recapitulated important facets of
503 human *P. falciparum* infection while allowing for a greater degree of control over critical experimental and
504 population variables. In particular, although our CHMI study employed narrowly defined parameters for

505 recruitment[24], there remained a strong potential for unassessed genetic, nutritional, and social factors
506 which may have contributed to microbiota variability amongst human participants, even before study
507 enrollment and *P. falciparum* infection. This created a challenge for determining whether the differences
508 we observed in baseline GI microbiota composition were a proxy for some other aspect of *P. falciparum*
509 susceptibility, or alternatively, played a direct role in risk for more severe infection. Our use of the RM
510 model allowed us to overcome some of these challenges, including the reduction of social, economic,
511 and medical confounders that are common amongst human cohorts. Additionally, while diet is a major
512 contributor to GI microbiota composition in both humans and RMs[43], the RMs included in this study were
513 fed a standardized diet of commercial primate chow in combination with additional fruits and vegetables,
514 all of which were provided daily. Thus, while animal-to-animal differences in GI microbiota composition
515 prior to *P. fragile* challenge were expected, this variability is unlikely to indicate unappreciated
516 comorbidities or other factors that may have influenced the outcome of *P. fragile* infection. Moreover,
517 the ability to stratify RMs according to their pre-infection microbiota composition without the added
518 complications of needing to account for diet or other population-specific confounders, not only
519 strengthens our observation of a significant role of the GI microbiome in protection against severe
520 *Plasmodium* infection but verifies the value of this critical model system for the examination of
521 *Plasmodium*-microbiome interactions.
522
523 Another major strength of our study was the use of an analytical approach that leveraged divisive
524 hierarchal clustering, as opposed to agglomerative, which enhanced our ability to segregate microbiota
525 communities into meaningful clusters. The ability to then identify stepwise increases in peak parasite
526 burdens across these microbiota clusters allowed us to not only verify previous murine and human
527 children and infant observational studies suggesting an association between the microbiome and the
528 magnitude of *Plasmodium* infection, but to extend these findings to a human adult cohort, as well as a
529 physiologically relevant RM model system. In sum, the data presented here and our specific bioinformatic
530 approach confirms the generalizability of our observations beyond specific participant populations, as
531 well as to other host and *Plasmodium* species.
532

533 In summary, the data presented here demonstrates that preexisting GI microbiome composition is highly
534 indicative of *Plasmodium* disease progression in both humans and RMs. Our findings decisively support
535 the existence of a broad link between GI microbiome communities and *Plasmodium* infection severity,
536 and also represent a critical extension of previous murine and human children and infant studies[19-23] into
537 adult human populations. Our ability to recapitulate this phenomenon in a relevant RM model also
538 expands the ability to perform mechanistic investigations of microbiota-influenced anti-malarial immunity.
539 While our current study is limited in its ability to make mechanistic determinations of the means by which
540 the GI microbiome contributes to protection against severe malaria, the identification of high-level
541 taxonomic differences in both human and RM cohorts suggests that microbiome targeting therapies, such
542 as microbiome modulation or small molecule supplementation, could be investigated to mitigate the
543 severity of *Plasmodium* infection. Taken together, our data provide a strong foundation for future RM and
544 human studies to not only identify the functional role of distinct microbial communities in controlling
545 malaria severity, but to pre-clinically test preventative and interventional strategies leveraging the
546 microbiome to reduce the burden of malaria.
547

548 **Acknowledgements**
549 We thank the individuals that participated in the KAF156 CHMI study. We thank all veterinary and
550 research support group staff of the Washington National Primate Research Center (WaNPRC) for their
551 aid with the RM study. We thank Dr. Sheri Hild for her support of these studies.
552

553 **Financial support**
554 This work was supported by grant K01OD024876 to JAM, who was further supported in part by grants
555 R21OD031435, R01HD108015, R01DA054553, and NIH base grant P51OD011104 to the Tulane
556 National Primate Research Center. The research was additionally supported in part by WaNPRC NIH
557 core grant P51OD010425. The KAF156 CHMI study was supported by Novartis.
558

559 **Author contributions**

560 JAM conceived of the study, oversaw the planning of the project, performed experiments, interpreted the
561 data, and wrote the paper. ATG assisted with sample collection from the RM study, analyzed and
562 interpreted the 16s rRNA sequencing data, and wrote the paper. CAB assisted with sample collection
563 from the RM study and performed the DNA extractions and 16s rRNA sequencing for both the RM and
564 CHMI studies. EC provided support for sample processing from the RM study. SW, NI, CYA, and WDG
565 provided research support for the RM study. KAG provided veterinary support for the RM study. KDP
566 provided the initial *P. fragile* stock. MG and NRK assisted with data interpretation and paper preparation.
567 JGK led and provided samples from the KAF156 CHMI study, assisted with data interpretation and paper
568 preparation.
569

570 **Conflicts of interest**

571 All authors report no potential conflicts of interest.
572

573 **Figure legends**

574 **Figure 1. Unsupervised hierarchical clustering of 16s rRNA sequencies identifies association**
575 **between GI microbiota composition and risk of severe *P. falciparum* parasitemia.** (A)
576 Representative timeline depicting CHMI sample collection schedule. CHMI participants provided stool
577 samples near *P. falciparum* challenge (between days -2 – 2), at peak parasitemia near when treatment
578 was initiated (days 10 – 17), post-treatment (days 12 – 19), and at a follow-up visit (days 27 – 46). (B)
579 Divisive hierarchical clustering to identify major clusters in baseline microbiota samples. Major clusters
580 were defined as human cluster 1 (HC1; pink), human cluster 2 (HC2; brown) and human cluster 3 (HC3;
581 green). Branch tips indicate the parasitemia severity of each participant, which was based on detection
582 of peak parasite levels. (C) Odds ratio assessment to determine likelihood of participants within each
583 microbiota cluster progressing to severe parasitemia. (D) Log2-transformed parasitemia values for
584 participants in each microbiota cluster.
585

586 **Figure 2. High diversity GI microbiota is linked to likelihood of developing severe *P. falciparum***
587 **parasitemia.** (A) Principal component analysis (PCA) of CLR-transformed count data. Colors indicate

588 hierarchically determined microbiota clusters, with HC1 shown in pink, HC2 in brown, and HC3 in green.
589 (B) Replicate PCA shown in A, with colors identifying samples associated with parasite levels. Blue points
590 indicate mild parasitemia, while red points indicate severe parasitemia. (C) PCA of samples at baseline
591 only, with points representative of HC1 (pink), HC2 (brown), and HC3 (green). (D) PCA of samples at
592 baseline only with points shaded to represent severe (red) and mild (blue) parasitemia. (E) Total number
593 of unique ASVs observed within each microbiota cluster. (F) Shannon diversity scores for participant
594 samples at all time points, grouped by microbiota cluster. (G) Shannon diversity scores for participants
595 at all time points, grouped by parasitemia severity.
596
597 **Figure 3. Abundance of core taxa is reduced in participants likely to develop severe *P. falciparum***
598 **parasitemia.** (A) Prevalence of all ASVs that were detected in at least one third of samples from each
599 microbiota cluster. Statistical values indicate significant differences in prevalence as determined by a
600 proportionality test. * = $p<0.05$, **=$p<0.005$, ***=$p<0.0005$. (B) CLR-transformed abundance data for top
601 20 most prevalent ASVs, when detected. Statistical significance between HC1 and HC3 was conducted
602 using a Wilcoxon test, with results that remined significant following Bonferroni corrected boxed in
603 magenta. (C) Heatmap of CLR-transformed count data for all genera detected as differentially abundant
604 at the baseline time point, with hierarchical clustering of genera shown to the right. (D-H) CLR-
605 transformed counts for all baseline samples in select differentially abundant genera. (I) Smoothed
606 abundance data over time. Solid colored lines represent mean count levels. For panels A-B and D-I, HC1
607 is shown in pink, HC2 is shown in brown and HC3 is shown in green.
608
609 **Figure 4. Unsupervised hierarchical clustering of 16s rRNA sequences identifies association**
610 **between GI microbiota composition and risk of severe *P. fragile* parasitemia.** (A) Representative
611 timeline depicting RM sample collection schedule. RM stool samples were collected twice prior to
612 challenge, then each of the next four weeks, with final follow-up at six weeks post-challenge. (B) Divisive
613 hierarchical clustering to identify major clusters in baseline microbiota samples. Branch tips indicate the
614 parasitemia severity of each macaque, which was based on peak detection. (C) Log2-transformed
615 parasitemia values for macaques in each microbiota cluster.

616

617 **Figure 5. GI microbiota composition linked to likelihood of developing severe *P. fragile***
618 **parasitemia.** (A) Principal Coordinate Analysis (PCoA) weighted-unifrac distances between samples.
619 Colors indicate hierarchically determined microbiota clusters, with MaC1 shown in pink and MaC2 shown
620 in green. (B) Replicate PCoA shown in (A), with colors identifying samples associated with parasite levels.
621 Blue points indicate mild parasitemia, while red points indicate severe parasitemia. (C) PCoA of samples
622 faceted by timepoint and colored by microbiota cluster.

623

624 **Figure 6. Abundance of core taxa reduced in macaques likely to develop severe *P. fragile***
625 **parasitemia.** (A) Prevalence of all ASVs that were detected in at least one third of samples from each
626 microbiota cluster. Statistical values indicate significant differences in prevalence as determined by a
627 proportionality test. * = $p<0.05$, **=$p<0.005$, ***=$p<0.0005$. (B) CLR-transformed abundance data for top
628 28 most prevalent ASVs, when detected. Statistical significance between HC1 and HC3 was conducted
629 using a Wilcoxon test, with results that remined significant following Bonferroni corrected boxed in
630 magenta. (C) Heatmap of CLR-transformed count data for all genera detected as differentially abundant
631 at the baseline time point, with hierarchical clustering of genera shown to the right. (D-E) CLR-
632 transformed counts for all baseline samples in select differentially abundant genera. (F) Smoothed
633 abundance data over time. Solid colored lines represent mean count levels. For panels A-B and D-F,
634 MaC1 is shown in pink, MaC2 is shown in green.

635

636 **Fig. S1. High diversity human GI microbiota linked to likelihood of developing severe *P.***
637 ***falciparum* parasitemia.** (A) Three-dimensional principal component analysis (PCA) of CLR-
638 transformed count data, with colors identifying samples associated with parasite levels. Blue points
639 indicate mild parasitemia, while red points indicate severe parasitemia. (B) Replicate PCA shown in (A),
640 with colors indicating hierarchically determined microbiota clusters. HC1 is shown in pink, HC2 is shown
641 in brown and HC3 is shown in green.

642

Fig. S2. Alpha diversity relates to parasite burden. (A) Linear model of parasite burden in relation to alpha diversity.

Fig. S3. High diversity macaque GI microbiota linked to likelihood of developing severe *P. falciparum* parasitemia. (A) Principal component analysis (PCA) of CLR-transformed count data. Colors indicate hierarchically determined microbiota clusters, with MaC1 shown in pink and MaC2 shown in green. (B) Replicate PCA shown in (A), with colors identifying samples associated with parasite levels. Blue points indicate mild parasitemia, while red points indicate severe parasitemia. (C) Shannon diversity scores for RM samples at all time points, grouped by microbiota cluster. (D) Shannon diversity scores for RM samples at all time points, grouped by parasitemia severity.

Fig. S4. Peak *P. fragile* parasite burdens varied across RMs. (A) *P. fragile* parasite detection in macaques over the study time course. Colors identify samples associated with parasite levels. Blue background indicates RMs with mild parasitemia, while red points indicate RMs that experienced severe parasitemia.

References

1 WHO. Vol. Licence: CC BY-NC-SA 3.0 IGO (ed WHO) (World Health Organization, Geneva, Switzerland, 2021).

2 Sowunmi, A., Ogundahunsi, O. A., Falade, C. O., Gbotosho, G. O. & Oduola, A. M. Gastrointestinal manifestations of acute falciparum malaria in children. *Acta tropica* **74**, 73-76 (2000).

3 Seydel, K. B., Milner, D. A., Jr., Kamiza, S. B., Molyneux, M. E. & Taylor, T. E. The distribution and intensity of parasite sequestration in comatose Malawian children. *The Journal of infectious diseases* **194**, 208-205, doi:10.1086/505078 (2006).

4 Pongponratn, E., Riganti, M., Punpoowong, B. & Aikawa, M. Microvascular sequestration of parasitized erythrocytes in human falciparum malaria: a pathological study. *The American journal of tropical medicine and hygiene* **44**, 168-175 (1991).

5 Mooney, J. P. *et al.* Inflammation-associated alterations to the intestinal microbiota reduce colonization resistance against non-typhoidal Salmonella during concurrent malaria parasite infection. *Scientific reports* **5**, 14603, doi:10.1038/srep14603 (2015).

6 Milner, D. A., Jr. *et al.* Quantitative Assessment of Multiorgan Sequestration of Parasites in Fatal Pediatric Cerebral Malaria. *The Journal of infectious diseases* **212**, 1317-1321, doi:10.1093/infdis/jiv205 (2015).

7 Olsson, R. A. & Johnston, E. H. Histopathologic changes and small-bowel absorption in falciparum malaria. *The American journal of tropical medicine and hygiene* **18**, 355-359 (1969).

8 Wilairatana, P., Meddings, J. B., Ho, M., Vannaphan, S. & Looareesuwan, S. Increased gastrointestinal permeability in patients with Plasmodium falciparum malaria. *Clinical infectious diseases : an official publication of the Infectious Diseases Society of America* **24**, 430-435 (1997).
9 Karney, W. W. & Tong, M. J. Malabsorption in Plasmodium falciparum malaria. *The American journal of tropical medicine and hygiene* **21**, 1-5 (1972).
10 Molyneux, M. E. *et al.* Reduced hepatic blood flow and intestinal malabsorption in severe falciparum malaria. *The American journal of tropical medicine and hygiene* **40**, 470-476 (1989).
11 Church, J. A., Nyamako, L., Olupot-Olupot, P., Maitland, K. & Urban, B. C. Increased adhesion of Plasmodium falciparum infected erythrocytes to ICAM-1 in children with acute intestinal injury. *Malaria Journal* **15**, 54, doi:10.1186/s12936-016-1110-3 (2016).
12 Chau, J. Y. *et al.* Malaria-associated L-arginine deficiency induces mast cell-associated disruption to intestinal barrier defenses against nontyphoidal Salmonella bacteremia. *Infection and immunity* **81**, 3515-3526, doi:10.1128/iai.00380-13 (2013).
13 Olupot-Olupot, P. *et al.* Endotoxaemia is common in children with Plasmodium falciparum malaria. *BMC infectious diseases* **13**, 117, doi:10.1186/1471-2334-13-117 (2013).
14 Berkley, J. A. *et al.* HIV infection, malnutrition, and invasive bacterial infection among children with severe malaria. *Clinical infectious diseases : an official publication of the Infectious Diseases Society of America* **49**, 336-343, doi:10.1086/600299 (2009).
15 Bronzan, R. N. *et al.* Bacteremia in Malawian children with severe malaria: prevalence, etiology, HIV coinfection, and outcome. *The Journal of infectious diseases* **195**, 895-904, doi:10.1086/511437 (2007).
16 Alamer, E. *et al.* Dissemination of non-typhoidal Salmonella during Plasmodium chabaudi infection affects anti-malarial immunity. *Parasitol Res* **118**, 2277-2285, doi:10.1007/s00436-019-06349-z (2019).
17 Potts, R. A. *et al.* Mast cells and histamine alter intestinal permeability during malaria parasite infection. *Immunobiology* **221**, 468-474, doi:10.1016/j.imbio.2015.11.003 (2016).
18 Roth, A. N., Grau, K. R. & Karst, S. M. Diverse Mechanisms Underlie Enhancement of Enteric Viruses by the Mammalian Intestinal Microbiota. *Viruses* **11**, 760 (2019).
19 Mandal, R. K. *et al.* Dynamic modulation of spleen germinal center reactions by gut bacteria during Plasmodium infection. *Cell Rep* **35**, 109094, doi:10.1016/j.celrep.2021.109094 (2021).
20 Yooseph, S. *et al.* Stool microbiota composition is associated with the prospective risk of Plasmodium falciparum infection. *BMC genomics* **16**, 631, doi:10.1186/s12864-015-1819-3 (2015).
21 Villarino, N. F. *et al.* Composition of the gut microbiota modulates the severity of malaria. *Proceedings of the National Academy of Sciences of the United States of America* **113**, 2235-2240, doi:10.1073/pnas.1504887113 (2016).
22 Taniguchi, T. *et al.* Plasmodium berghei ANKA causes intestinal malaria associated with dysbiosis. *Scientific reports* **5**, 15699, doi:10.1038/srep15699 (2015).
23 Waide, M. L. *et al.* Gut Microbiota Composition Modulates the Magnitude and Quality of Germinal Centers during Plasmodium Infections. *Cell Rep* **33**, 108503, doi:10.1016/j.celrep.2020.108503 (2020).
24 Kublin, J. G. *et al.* Safety, Pharmacokinetics, and Causal Prophylactic Efficacy of KAF156 in a Plasmodium falciparum Human Infection Study. *Clinical infectious diseases : an official publication of the Infectious Diseases Society of America* **73**, e2407-e2414, doi:10.1093/cid/ciaa952 (2021).
25 Murphy, S. C., Daza, G., Chang, M. & Coombs, R. Laser cutting eliminates nucleic acid cross-contamination in dried-blood-spot processing. *Journal of clinical microbiology* **50**, 4128-4130, doi:10.1128/jcm.02549-12 (2012).
26 Seilie, A. M. *et al.* Beyond Blood Smears: Qualification of Plasmodium 18S rRNA as a Biomarker for Controlled Human Malaria Infections. *The American journal of tropical medicine and hygiene* **100**, 1466-1476, doi:10.4269/ajtmh.19-0094 (2019).
27 (Manassas, Virginia, 2013).
28 Lim, C. *et al.* Improved light microscopy counting method for accurately counting Plasmodium parasitemia and reticulocytemia. *Am J Hematol* **91**, 852-855, doi:10.1002/ajh.24383 (2016).

29 Walters, W. *et al.* Improved Bacterial 16S rRNA Gene (V4 and V4-5) and Fungal Internal Transcribed Spacer Marker Gene Primers for Microbial Community Surveys. *mSystems* **1**, doi:10.1128/mSystems.00009-15 (2016).
30 Caporaso, J. G. *et al.* Global patterns of 16S rRNA diversity at a depth of millions of sequences per sample. *Proceedings of the National Academy of Sciences* **108**, 4516, doi:10.1073/pnas.1000080107 (2011).
31 Dissanaike, A., Nelson, P. & Garnham, P. Two New Malaria Parasites, *Plasmodium cynomolgi ceylonesis* subsp. nov and *Plasmodium fragile* sp. nov., from Monkeys in Ceylon. *Ceylon Journal of Medical Research*, 717-721 (1965).
32 Collins, W. E. *et al.* Studies on sporozoite-induced and chronic infections with Plasmodium fragile in Macaca mulatta and New World monkeys. *J Parasitol* **92**, 1019-1026, doi:10.1645/ge-848r.1 (2006).
33 Collins, W. E., Chin, W. & Skinner, J. C. Plasmodium fragile and Macaca mulatta monkeys as a model system for the study of malaria vaccines. *The American journal of tropical medicine and hygiene* **28**, 948-954, doi:10.4269/ajtmh.1979.28.948 (1979).
34 Abt, M. C. *et al.* Commensal bacteria calibrate the activation threshold of innate antiviral immunity. *Immunity* **37**, 158-170, doi:10.1016/j.immuni.2012.04.011 (2012).
35 Brown, R. L., Sequeira, R. P. & Clarke, T. B. The microbiota protects against respiratory infection via GM-CSF signaling. *Nature communications* **8**, 1512, doi:10.1038/s41467-017-01803-x (2017).
36 Ganal, S. C. *et al.* Priming of natural killer cells by nonmucosal mononuclear phagocytes requires instructive signals from commensal microbiota. *Immunity* **37**, 171-186, doi:10.1016/j.immuni.2012.05.020 (2012).
37 Hensley-McBain, T. *et al.* Increased mucosal neutrophil survival is associated with altered microbiota in HIV infection. *PLoS pathogens* **15**, e1007672, doi:10.1371/journal.ppat.1007672 (2019).
38 Rooks, M. G. & Garrett, W. S. Gut microbiota, metabolites and host immunity. *Nat Rev Immunol* **16**, 341-352, doi:10.1038/nri.2016.42 (2016).
39 Mandal, R. K. *et al.* Longitudinal Analysis of Infant Stool Bacteria Communities Before and After Acute Febrile Malaria and Artemether-Lumefantrine Treatment. *The Journal of infectious diseases* **220**, 687-698, doi:10.1093/infdis/jiy740 (2019).
40 Guan, W. *et al.* Observation of the Gut Microbiota Profile in BALB/c Mice Induced by Plasmodium yoelii 17XL Infection. *Frontiers in microbiology* **13**, 858897, doi:10.3389/fmicb.2022.858897 (2022).
41 Guan, W. *et al.* Observation of the Gut Microbiota Profile in C57BL/6 Mice Induced by Plasmodium berghei ANKA Infection. *Frontiers in cellular and infection microbiology* **11**, 680383, doi:10.3389/fcimb.2021.680383 (2021).
42 Fan, Z. G. *et al.* Gut Microbiota Reconstruction Following Host Infection with Blood-stage Plasmodium berghei ANKA Strain in a Murine Model. *Curr Med Sci* **39**, 883-889, doi:10.1007/s11596-019-2119-y (2019).
43 Zmora, N., Suez, J. & Elinav, E. You are what you eat: diet, health and the gut microbiota. *Nature reviews. Gastroenterology & hepatology* **16**, 35-56, doi:10.1038/s41575-018-0061-2 (2019).

Figure 1

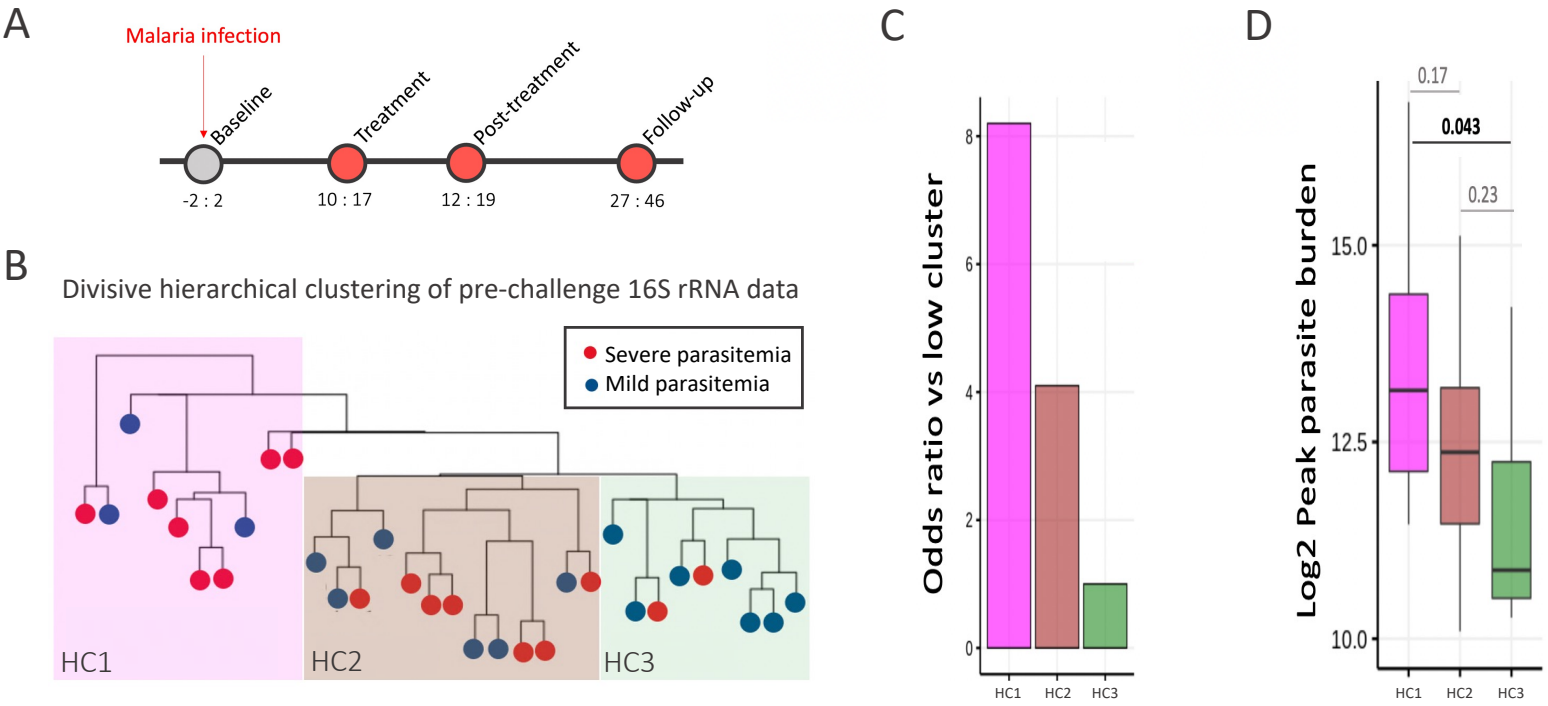
A
Malaria infection
Baseline
Treatment
Post-treatment
Follow-up
-2 : 2
10 : 17
12 : 19
27 : 46
B
Divisive hierarchical clustering of pre-challenge 16S rRNA data
Severe parasitemia
Mild parasitemia
HC1
HC2
HC3
C
Odds ratio vs low cluster
0
2
4
6
8
HC1
HC2
HC3
D
Log2 Peak parasite burden
10.0
12.5
15.0
0.17
0.043
0.23
HC1
HC2
HC3

Figure 2

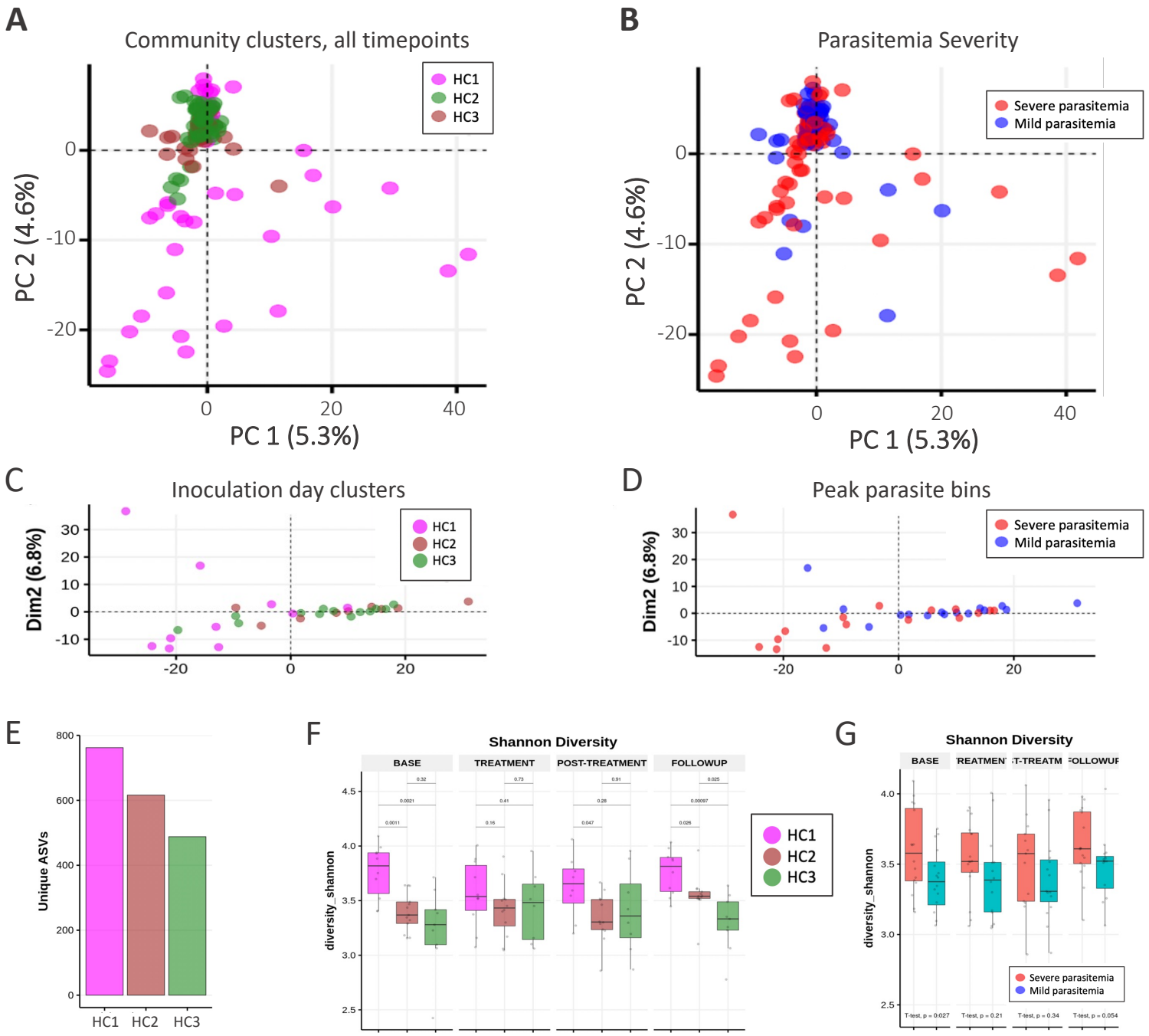
A
Community clusters, all timepoints
HC1
HC2
HC3
PC 2 (4.6%)
PC 1 (5.3%)
B
Parasitemia Severity
Severe parasitemia
Mild parasitemia
PC 2 (4.6%)
PC 1 (5.3%)
C
Inoculation day clusters
HC1
HC2
HC3
Dim2 (6.8%)
D
Peak parasite bins
Severe parasitemia
Mild parasitemia
Dim2 (6.8%)
E
Unique ASVs
HC1
HC2
HC3
F
Shannon Diversity
BASE
TREATMENT
POST-TREATMENT
FOLLOWUP
diversity_shannon
HC1
HC2
HC3
G
Shannon Diversity
BASE
diversity_shannon
Severe parasitemia
Mild parasitemia

Figure 3

A
ASVS detected in at least 1/3 of samples from either HC1 (pink) or HC3 (green)
p-value < 0.05 *
p-value < 0.005 **
p-value < 0.0005 ***
HC1
HC3
Prevalence within clusters
100%
75%
50%
25%
0%
B
HC1
HC2
HC3
C
CLR counts
Bifidobacterium
Blautia
Streptococcus
Roseburia
Escherichia
Catenibacterium
Megasphaera
WAL_1855D
Peptoniphilus
Megamonas
HC1
HC2
HC3
D
Bifidobacterium
E
Streptococcus
F
Megamonas
G
Escherichia
H
Catenibacterium
value
I
Megamonas
Bifidobacterium
Blautia
Streptococcus
Roseburia
Escherichia
Catenibacterium
Megasphaera
Peptoniphilus
WAL_1855D
Study start
Study conclusion

Figure 4

A

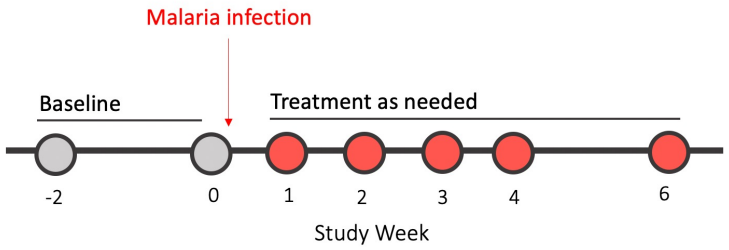
Malaria infection
Baseline
Treatment as needed
-2
0
1
2
3
4
6
Study Week

B

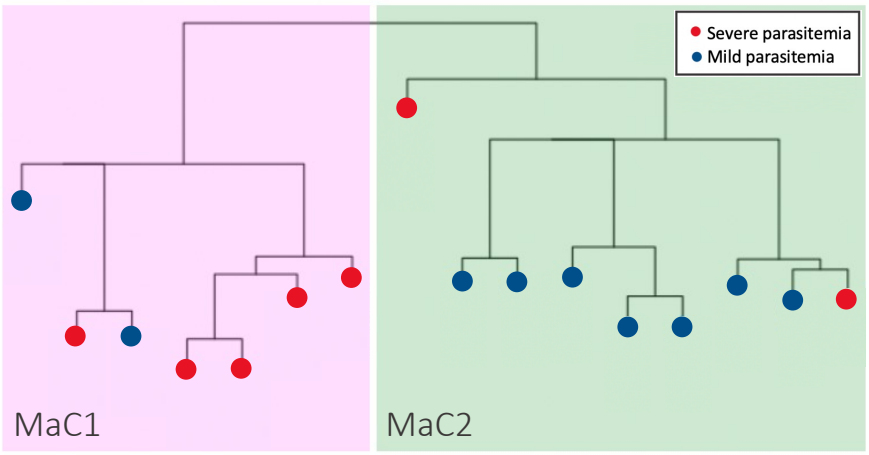
Divisive hierarchical clustering of pre-challenge 16S rRNA data
Severe parasitemia
Mild parasitemia
MaC1
MaC2

C

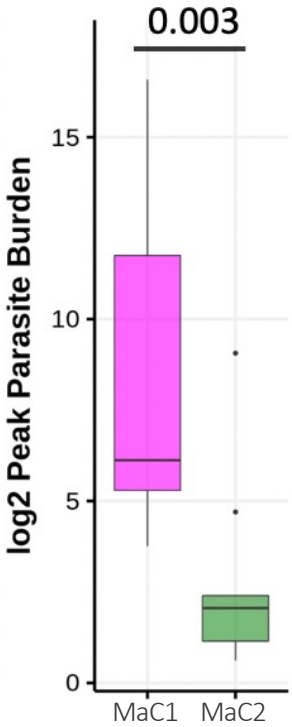
0.003
log2 Peak Parasite Burden
15
10
5
0
MaC1
MaC2

Figure 5

A

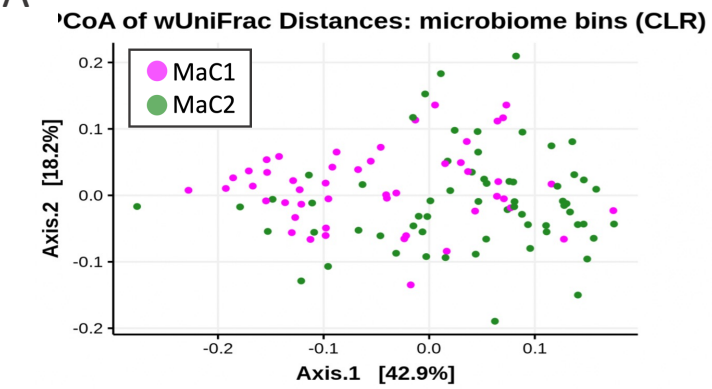
PCoA of wUniFrac Distances: microbiome bins (CLR)
MaC1
MaC2
Axis.2 [18.2%]
Axis.1 [42.9%]
0.2
0.1
0.0
-0.1
-0.2
-0.2
-0.1
0.0
0.1

B

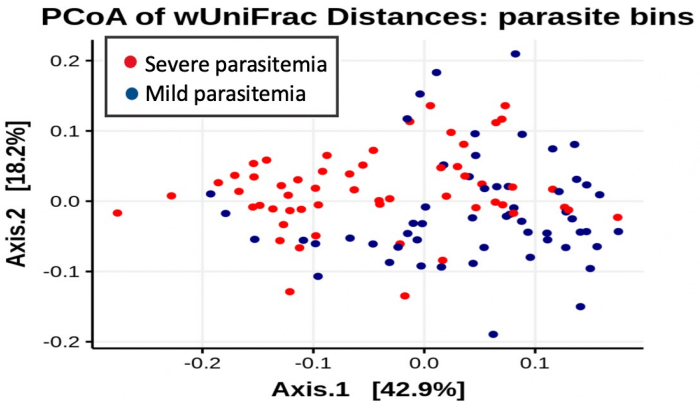
PCoA of wUniFrac Distances: parasite bins
Severe parasitemia
Mild parasitemia
Axis.2 [18.2%]
Axis.1 [42.9%]
0.2
0.1
0.0
-0.1
-0.2
-0.2
-0.1
0.0
0.1

C

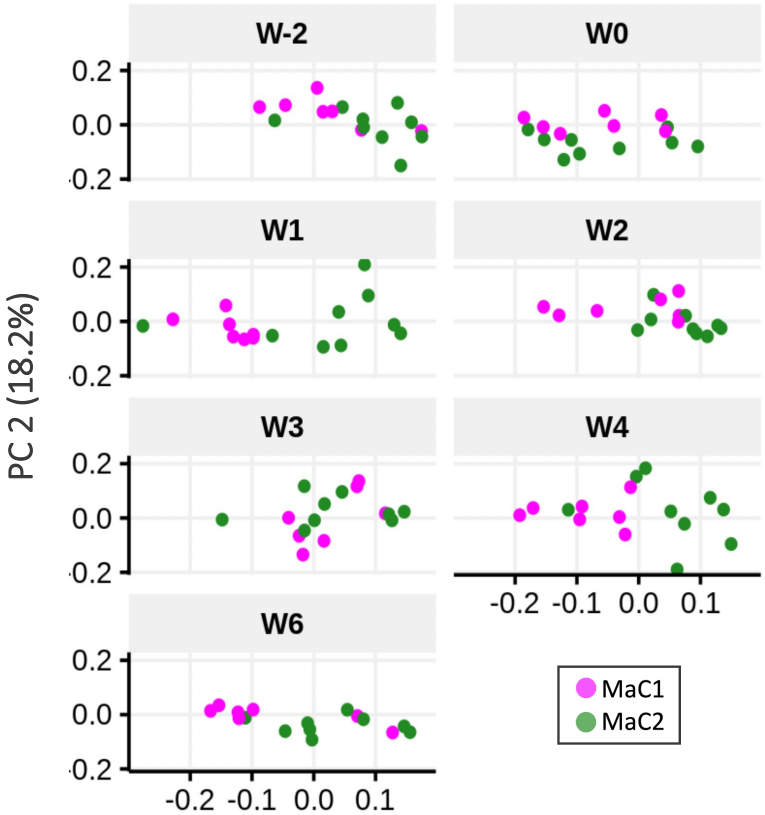
W-2
W0
W1
W2
W3
W4
W6
PC 2 (18.2%)
0.2
0.0
-0.2
-0.2
-0.1
0.0
0.1
MaC1
MaC2

Figure 6

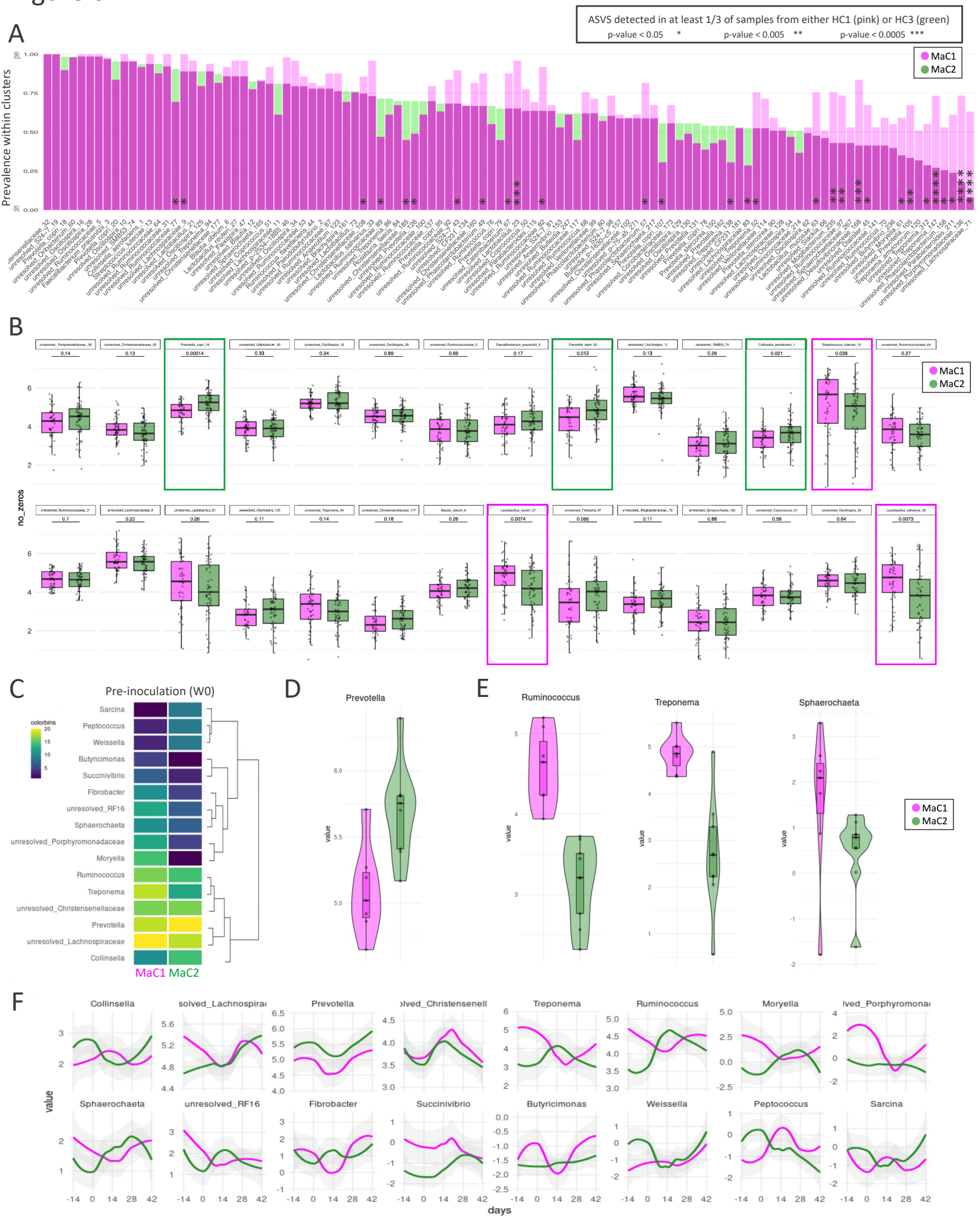
ASVS detected in at least 1/3 of samples from either HC1 (pink) or HC3 (green)
p-value < 0.05 *
p-value < 0.005 **
p-value < 0.0005 ***
A
Prevalence within clusters
MaC1
MaC2
B
no_zeros
MaC1
MaC2
C
Pre-inoculation (W0)
colorbins
Sarcina
Peptococcus
Weissella
Butyricimonas
Succinivibrio
Fibrobacter
unresolved_RF16
Sphaerochaeta
unresolved_Porphyromonadaceae
Moryella
Ruminococcus
Treponema
unresolved_Christensenellaceae
Prevotella
unresolved_Lachnospiraceae
Collinsella
MaC1 MaC2
D
Prevotella
value
E
Ruminococcus
Treponema
Sphaerochaeta
value
MaC1
MaC2
F
Collinsella
Prevotella
Treponema
Ruminococcus
Moryella
Sphaerochaeta
unresolved_RF16
Fibrobacter
Succinivibrio
Butyricimonas
Weissella
Peptococcus
Sarcina
value
days

Fig.S1

A

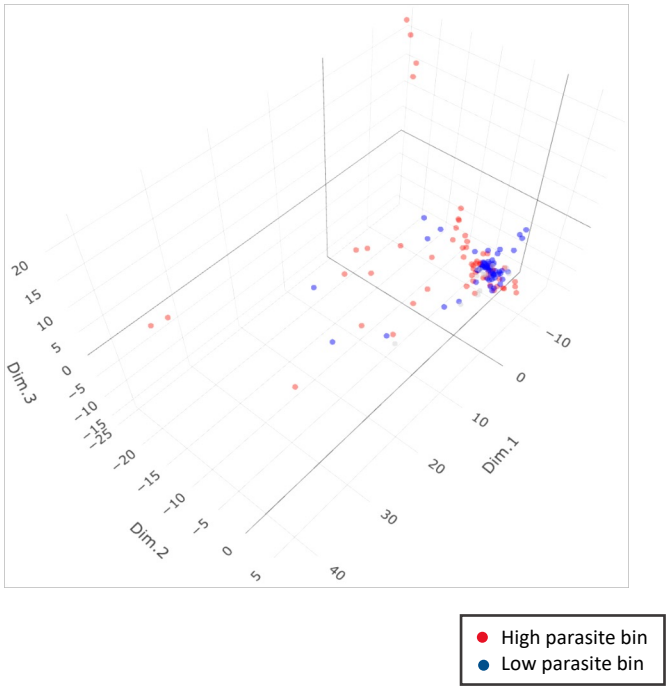
Dim.3
Dim.2
Dim.1
High parasite bin
Low parasite bin

B

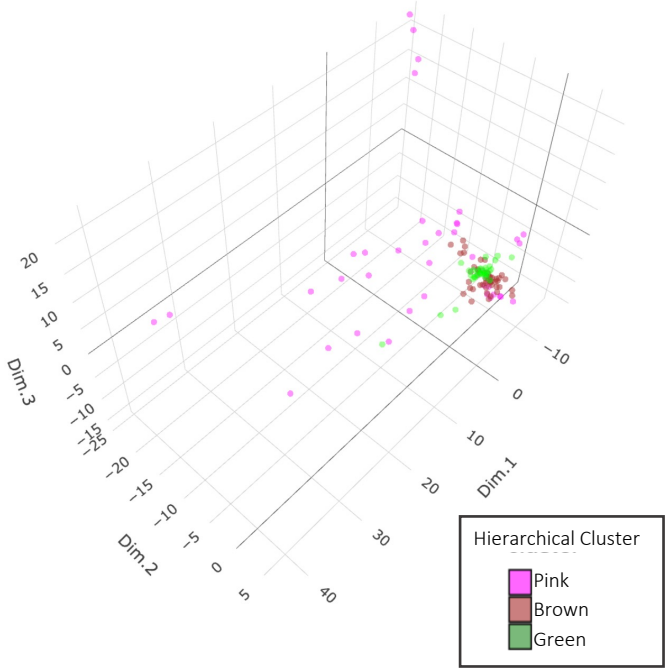
Dim.3
Dim.2
Dim.1
Hierarchical Cluster
Pink
Brown
Green

Fig.S2

A

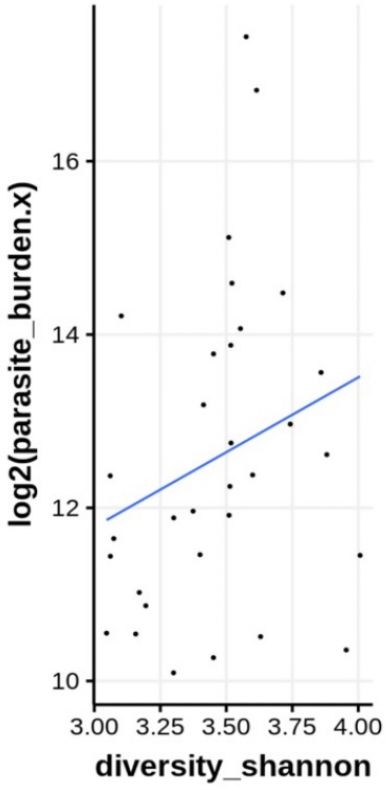
log2(parasite_burden.x)
16
14
12
10
3.00
3.25
3.50
3.75
4.00
diversity_shannon

Fig.S3

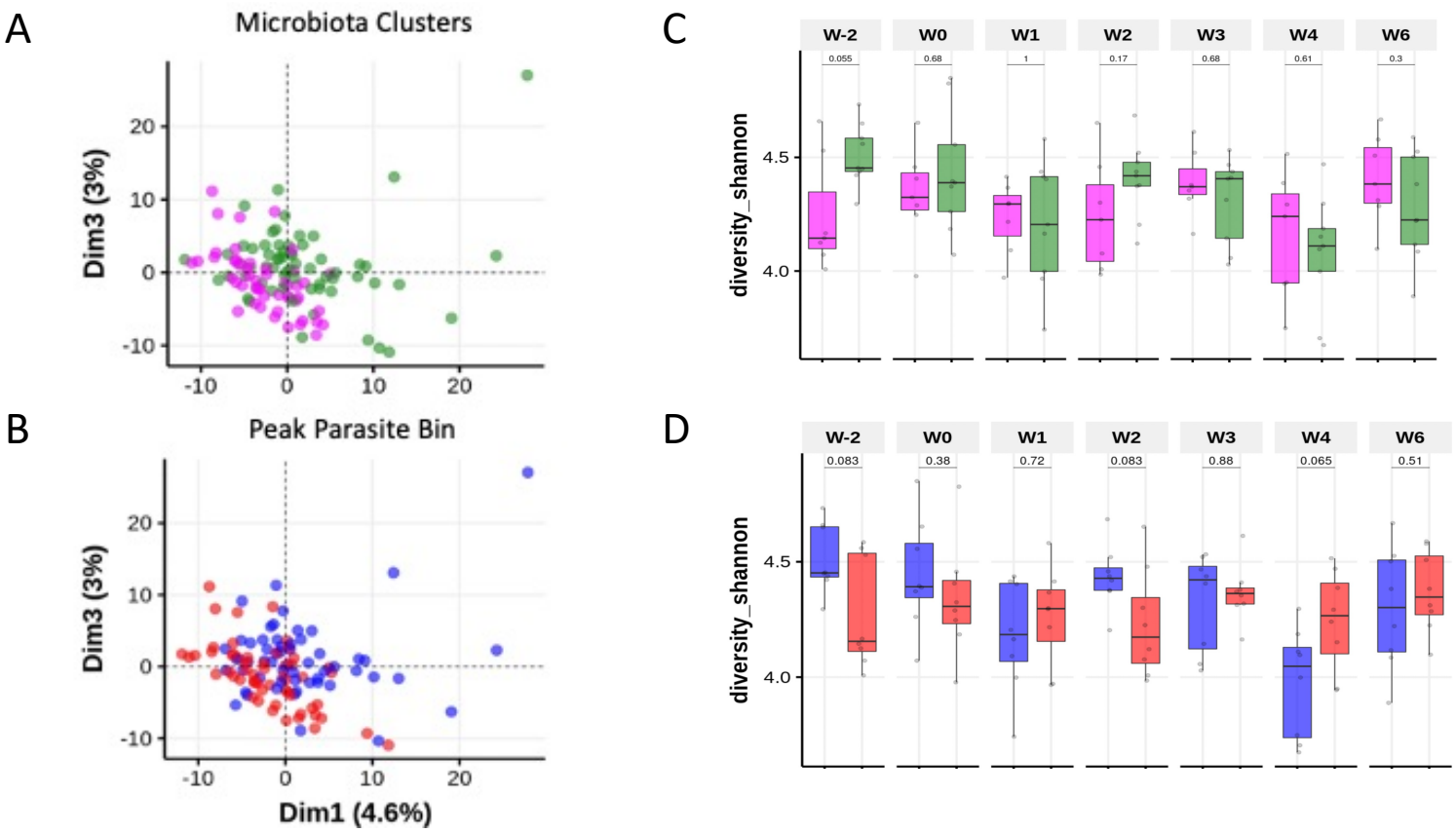
A
Microbiota Clusters
Dim3 (3%)
20
10
0
-10
-10
0
10
20
B
Peak Parasite Bin
Dim3 (3%)
20
10
0
-10
-10
0
10
20
Dim1 (4.6%)
C
W-2
W0
W1
W2
W3
W4
W6
0.055
0.68
1
0.17
0.68
0.61
0.3
diversity_shannon
4.5
4.0
D
W-2
W0
W1
W2
W3
W4
W6
0.083
0.38
0.72
0.083
0.88
0.065
0.51
diversity_shannon
4.5
4.0

Fig.S4

A

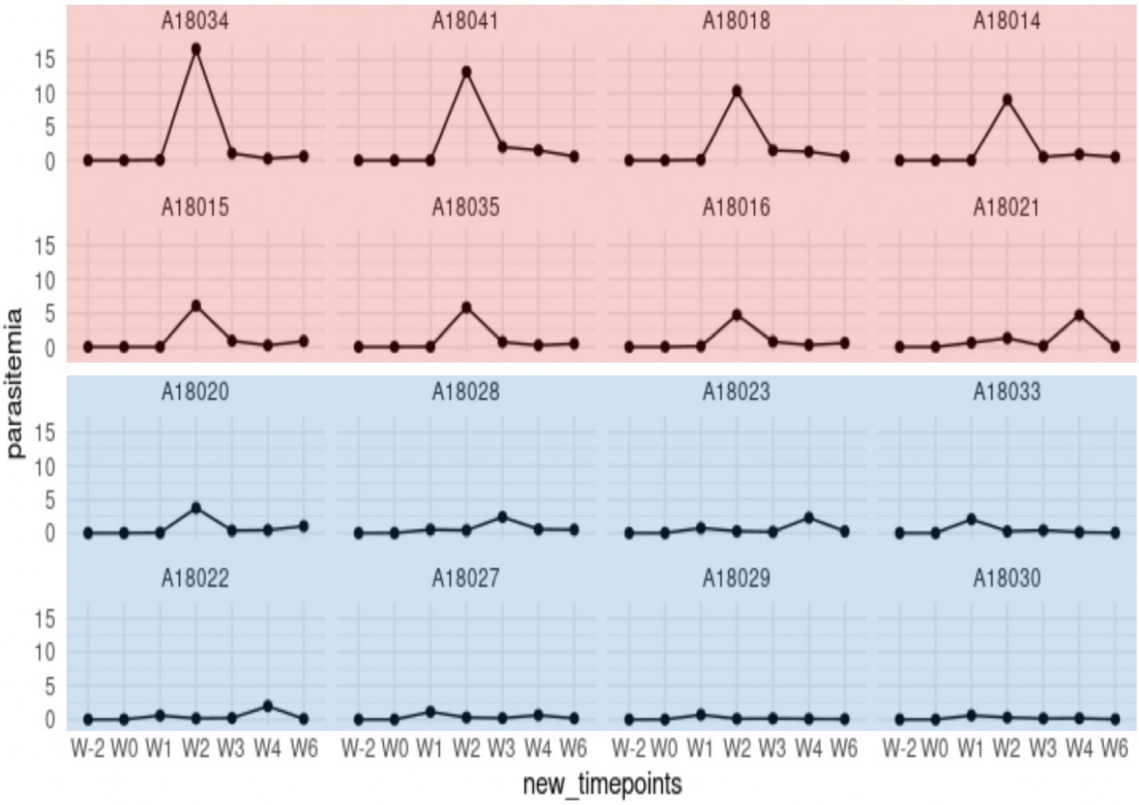
A18034
A18041
A18018
A18014
A18015
A18035
A18016
A18021
A18020
A18028
A18023
A18033
A18022
A18027
A18029
A18030
parasitemia
15
10
5
0
W-2 W0 W1 W2 W3 W4 W6
new_timepoints